Sensor and Simulation Notes

Note 465

March 2002

Development and Testing of a Parachute Deployable Impulse Radiating Antenna

Lanney M. Atchley and Everett G. Farr
Farr Research, Inc.

J. Scott Tyo
University of New Mexico

Noel de la Merced
Irvin Aerospace Inc.

Larry L. Altgilbers
U. S. Army SMDC

Abstract

We introduce here a new embodiment of the Impulse Radiating Antenna (IRA). This new design evolves from an existing Farr Research, Inc. Collapsible IRA (CIRA) modified to be parachute deployed with a self-contained transmitter and power source. Our goals are to evaluate the potential area coverage and field strength obtainable using a parachute IRA (Para-IRA) while developing prototype hardware and testing techniques.

Table of Contents

1. Introduction

We introduce here a new embodiment of the Impulse Radiating Antenna (IRA). This new design evolves from an existing Farr Research, Inc. Collapsible IRA (CIRA) modified to be parachute deployed with a self-contained transmitter and power source. Our goals are to evaluate the potential area coverage and field strength obtainable using a parachute IRA (Para-IRA) while developing prototype hardware and testing techniques.

A sketch of the overall concept of the Para-IRA is shown in Figure 1.1. The reflector has a diameter of 4 feet (1.22 m). The feed arms are fabricated from conductive ripstop nylon, and the parabolic reflector is fabricated from conductive mesh that is air permeable. Fabric resistors designed to damp out electric oscillations are placed where the feed arms attach to the reflector. The reflector is fabricated from a conductive mesh that is permeable to air, so the parachute, instead of the reflector, absorbs the bulk of the stresses. If the reflector absorbed the stresses, then it would tend to defocus the antenna.

A zipper balun, at the output of the transmitter, attempts to match the 50-ohm impedance of the transmitter output to the 200-ohm impedance of the antenna. Ideally the zipper should be several wavelengths long, in order to minimize reflections. But because there is limited space, we will likely have to settle for a shorter transition, resulting in a modest compromise in performance.

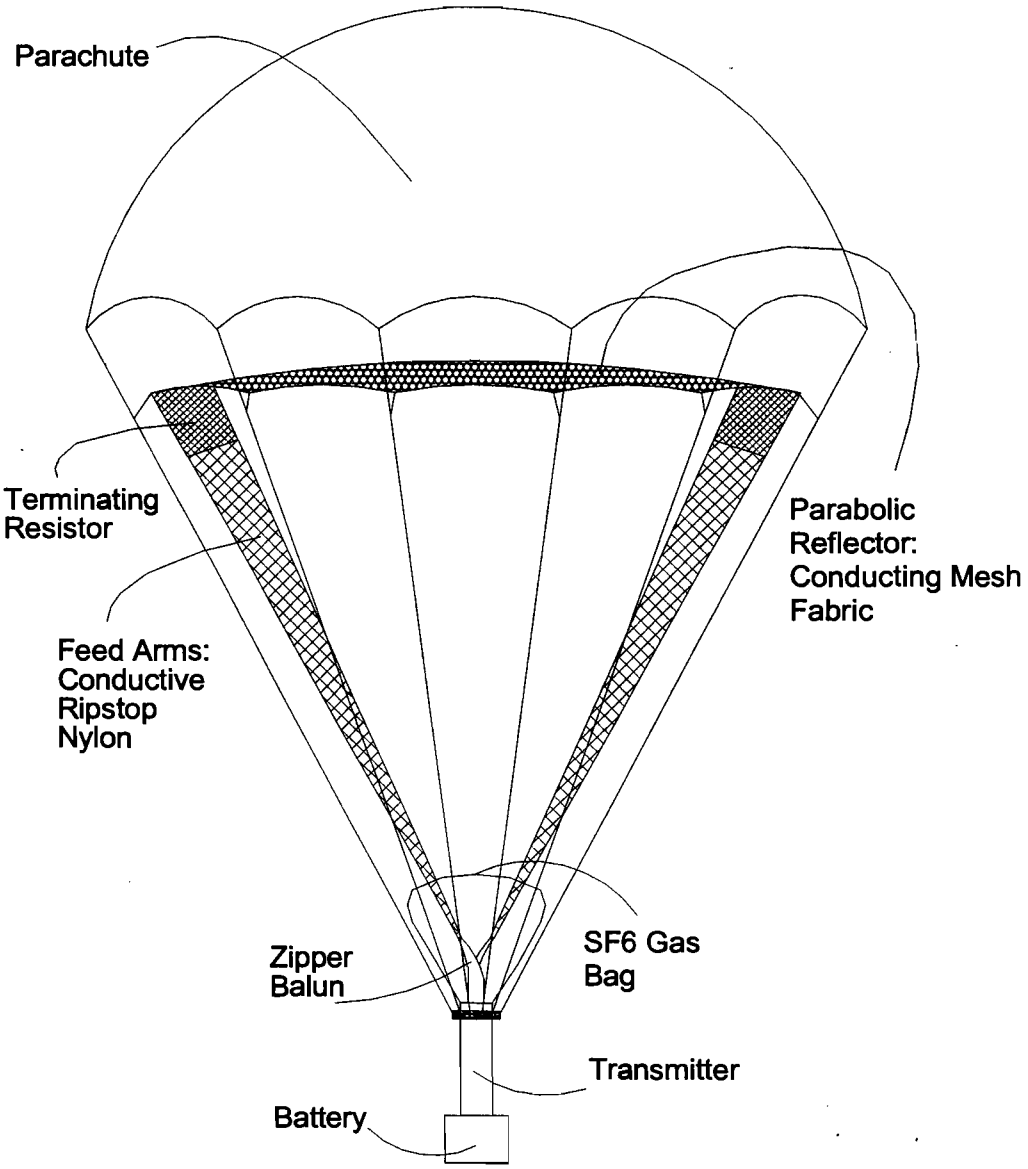

Figure 1.1. Para-IRA with parachute, antenna, balun, SF_6 gas bag, transmitter, and battery.

Two key parts of the RF system are the parachute and the antenna. Therefore, this project required expertise in both electromagnetics and aerodynamic engineering. For that reason, Farr Research teamed with Irvin Aerospace, one of the largest manufacturers of parachutes. Farr Research designed and evaluated the electromagnetic characteristics of the Para-IRA, and Irvin Aerospace advised on aerodynamic and packaging aspects of the complete Para-IRA.

We decided early in the project to separate the antenna reflector from the parachute canopy. In conversations with Irvin Aerospace, we learned that the air turbulence around a descending parachute canopy is too great to allow accurate control of the canopy curvature. By fabricating the reflector from a sparse conducting mesh fabric, we reduce air turbulence on the reflector. Furthermore, by suspending the reflector with radial tension from the parachute lines,

we expect to maintain a parabolic shape within a tolerance of ±2.5 cm. Irvin Aerospace modified an existing parachute, in order to produce a functional parachute suitable for mechanical and aerodynamic testing with the Farr Research prototype Para-IRA.

2. Technical Objectives

Our prime technical objective was to build and test a prototype antenna. We tested the antenna using a Farr Research time domain antenna range to evaluate the electromagnetic characteristics. This allowed us to determine the field strength and beamwidth radiated by the basic design. We varied the basic design to evaluate potential improvements. From our testing we are able to provide preliminary design information. We worked with parachute manufacturers to investigate the challenges of incorporating an antenna into a standard parachute design.

3. Technical Approach

3.1 Electromagnetic

Our technical approach was to fabricate a prototype Para-IRAs and test the important radiating parameters using Farr Research's time domain antenna range. We fabricated the electromagnetically functional prototype reflector from ripstop nylon. We backed the reflector with strips of Velcro, such that the reflector could be mounted either onto a parabolic wooden frame or inside a polycarbonate hoop frame. The wood frame provided a rigid support that forced the reflector into a parabolic shape. The hoop provided only radial support at the reflector circumference, allowing the reflector to be shaped by air pressure. In both cases, thin wooden struts supported the feed arms.

For the electromagnetic testing we used Farr Research's time domain antenna range. Using comparatively inexpensive instrumentation, this range allowed us to evaluate the critical antenna radiation parameters in a small indoors area. The technique uses time domain sampling and windowing to reduce cost and space requirements.

3.2 Aerodynamic

In collaboration with Irvin Aerospace, we designed a prototype parachute. This parachute was used to test the basic concept and aerodynamic parameters of the Para-IRA. The parachute was selected to provide the approximately correct descent rate, while being as small as possible for eventual packaging into a compact unit. Farr Research fabricated a mesh reflector to mate to the Irvin Aerospace parachute.

Our approach for the first aerodynamic test consisted of towing the parachute and mesh reflector behind a truck. We did this to ensure that the mesh reflector would inflate properly. In addition, we measured the force generated on the complete Para-IRA, to establish the relationship between weight and descent rate.

4. Prototype Para-IRA Description

4.1 Mesh Prototype

The first Phase I Para-IRA prototype reflector is a 48-inch (122 cm) octagon, with an F/D ratio of unity. The fabric was a metallized mesh from Swift Textile. This model has no feed arms because we used it only for aerodynamic testing – not for electromagnetic testing. The reflector, as installed in a 6-ft surplus parachute, is shown in Figure 4.1. Note that this parachute canopy is slightly too small, because it is a surplus parachute not designed specifically for this reflector.

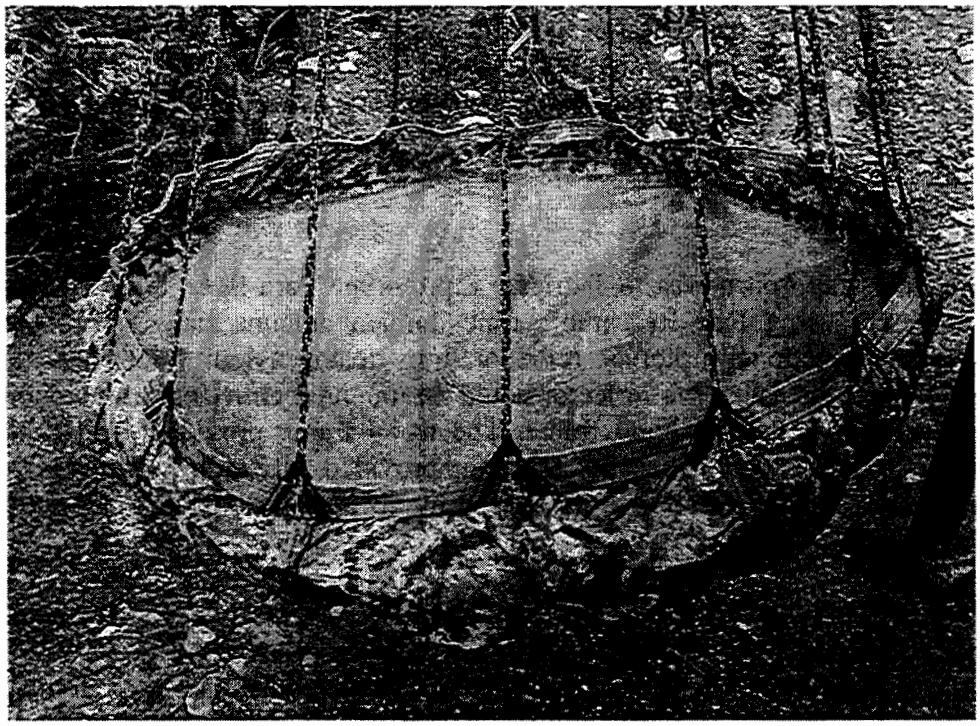

Figure 4.1. Prototype Mesh Para-IRA in surplus parachute.

4.2 Ripstop Nylon Prototype

We fabricated the second prototype from conductive ripstop nylon. It is a twelve-sided reflector complete with feed arms as shown from two perspectives in Figure 4.2. This prototype was used for all the electromagnetic testing. For the boresight and beamwidth measurements, we mounted the prototype on the wooden frame using Velcro. For the inflation test, the antenna was supported by a polycarbonate ring using Velcro straps attached at the periphery of the reflector.

Figure 4.3 shows the wooden frame and feed arm support without the reflector. We backed the reflector and the wooden frame with Velcro along the entire length of the gore seams. We did this so the reflector formed an accurate parabola when mounted on the frame. Figure 4.4 shows the reflector mounted on the polycarbonate ring using Velcro straps. The reflector is attached to the polycarbonate ring only at its periphery, thus allowing the reflector shape to be formed by air pressure during the inflation test.

4.3 Parachute

Irvin Aerospace's prototype parachute, shown in Figure 4.5, is a 6.6-ft. (2.0 m) diameter conical ribbon main parachute. This parachute is qualified and used on the Air Launch Cruise Missile (ALCM) flight termination system. The parachute was subjected to dynamic pressure as high as 970 pounds per square feet (46.4 kN/m^2). The parachute has been redesigned to reduce weight, due to lower canopy loading for this application. The reflector is attached to the parachute at the twelve gore seams so that it opens into its normal parabolic shape.

Figure 4.6 shows an artist's rendition of the parachute with attached IRA. The main parachute characteristics are as follows:

Nominal Diameter	(Do)	6.6 ft.	(2 m)
Nominal Area	(S)	34.21 $ft.^2$	(3.18 m^2)
Conical Angle	(μ)	25°	
Total Porosity	(λ)	18.9%	
Drag Coefficient	(C_d)	0.53	
Drag Area	(C_dS)	18.13 $ft.^2$	(1.68 m^2)
Number of Gores	(N)	12	
Suspension Line Length Ratio	(L_s/Do)	1.0	
Weight	(lbs)	3.50	(1.59 kg)

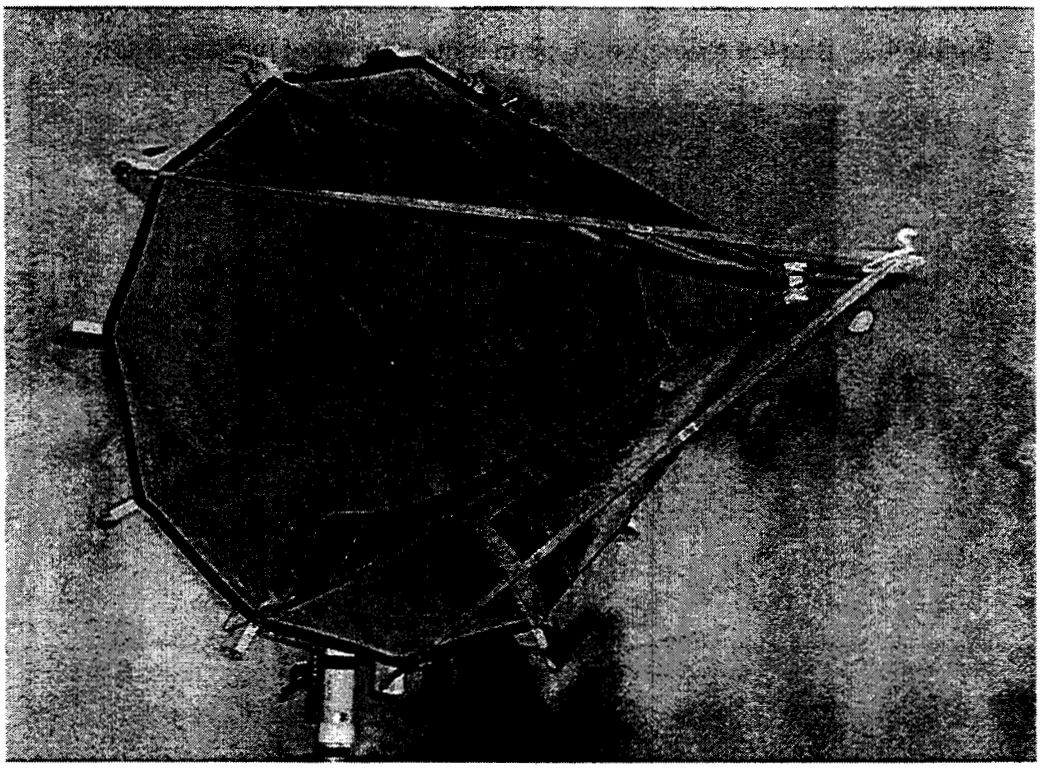

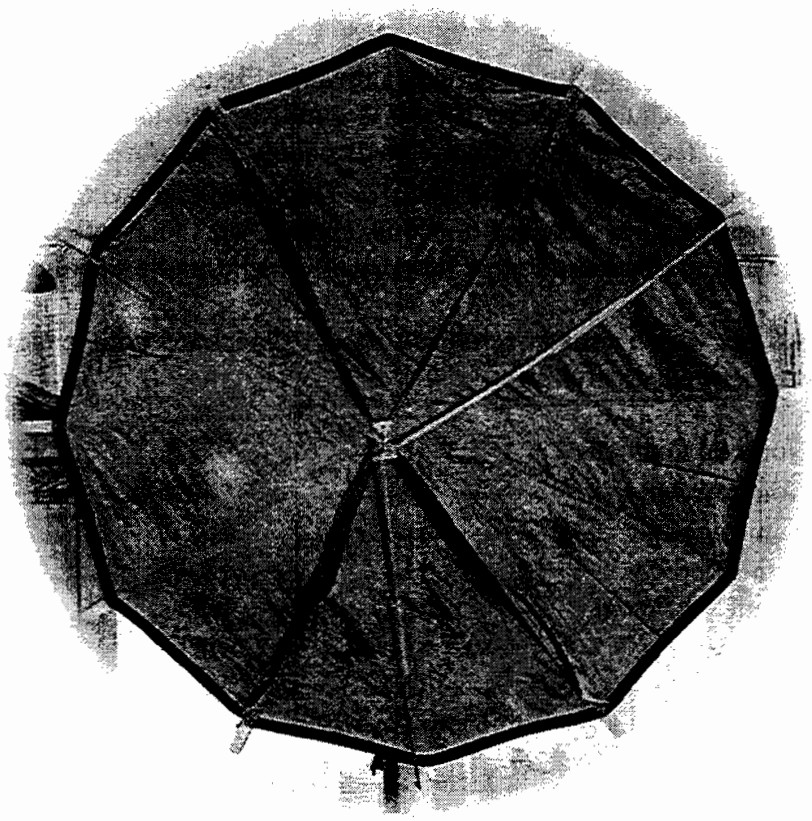

Figure 4.2. Ripstop nylon prototype mounted on wood backing frame.

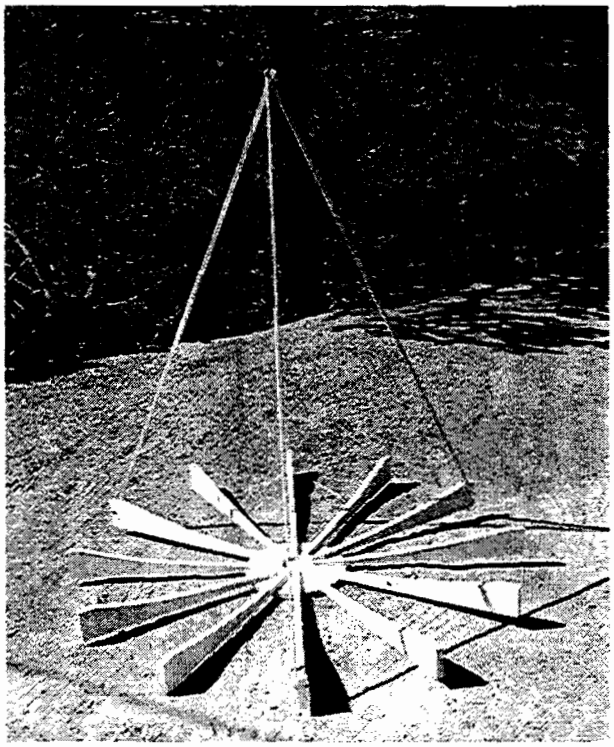

Figure 4.3. Wooden Frame for the Para-IRA.

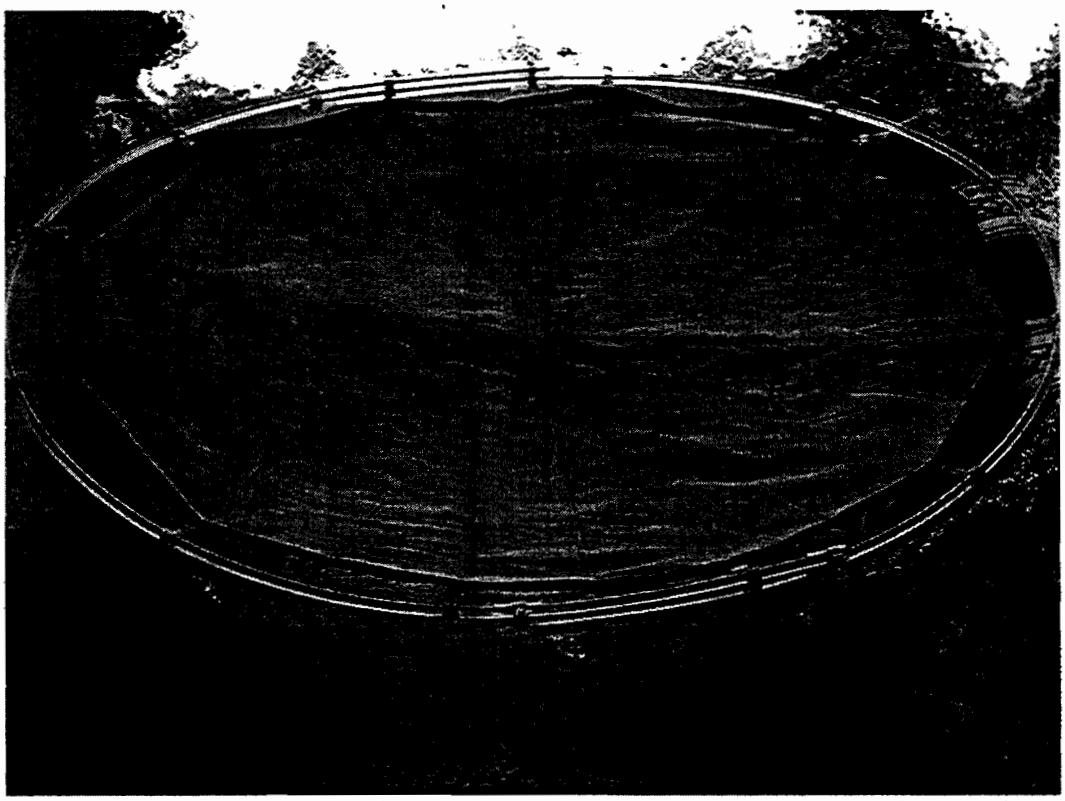

Figure 4.4. The Reflector of the Para-IRA as supported by a polycarbonate ring.

Figure 4.5. Irvin Aerospace's ribbon parachute with mesh CIRA.

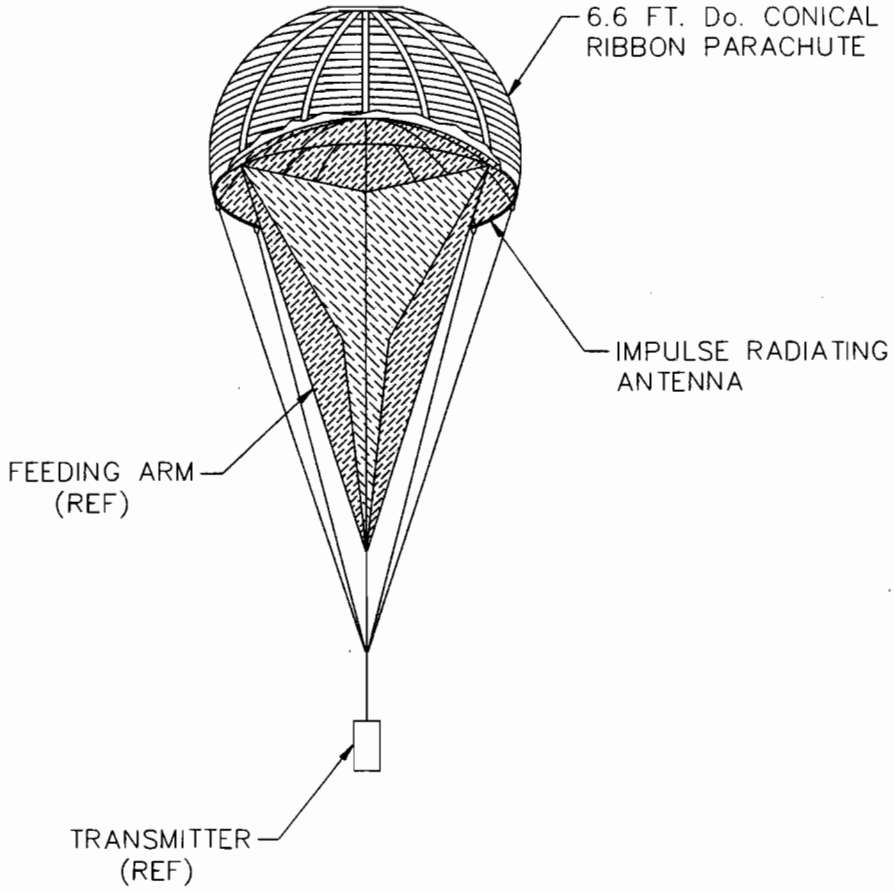

Figure 4.6. Main Parachute with Para-IRA antenna.

5. Descent Rate Calculation

We consider now the rate of descent for the Para-IRA. Given the weight of the submunition, we iterated between the size of the parachute and the descent rate. We sized our prototype parachutes to be as small as possible for compact packaging, while still allowing a sufficiently slow descent rate to allow the transmitter time to stabilize and operate.

We calculate the size of the parachute and it's descent rate. To a first approximation, we can write a relationship between the constant descent velocity of a solid round parachute and its size and total weight as [1]:

$$v \cong \sqrt{\frac{2w}{\rho k s}}$$

where:

v = parachute descent rate, m/s (ft/s)
w = mass of the parachute and load in kg (pounds)
k = parachute drag coefficient (~ 0.8 for a solid round parachute)
s = parachute surface area as projected flat, m^2 (ft^2)
ρ = 1.225 kg/m^3 (0.00237 sl/ft^3) at sea level
ρ = 1.07 kg/m^3 (0.00211 sl/ft^3) at 1219 m (4000 ft) above sea level.

Farr Research's existing CIRA has a diameter of four feet. For the CIRA to be suspended from the lines of a parachute at the parachute's skirt, the parachute is sized at two meters in diameter. From the above equation, for a 50-pound (22.7 kg) total weight, and lowering k to 0.6 to accommodate parachute venting, the descent velocity of the Para-IRA will be 45.3 feet per second (30.9 mph) (13.8 m/s). At that descent rate, the Para-IRA will take about 116 seconds to travel one mile (1.6 km). Thus there should be about a one and one-half minutes transmit window.

6. Electromagnetic Analysis

6.1 Boresight Electric Field

We provide here predictions of the field on boresight. The boresight electric field generated by the Para-IRA is determined from equations [2, equations 2.3 and 2.4] as:

$$E_{rad} = \frac{\tau\, a}{\sqrt{2}\,\pi\, r\, c\, f_g}\,\frac{dV}{dt}$$

where:

E_{rad} = radiated field (V/m)
τ = voltage transmission coefficient from the feed cable to the antenna, unitless (2)
a = reflector radius (0.61 m)
r = radial distance from the antenna (meters)
c = 3x10^8 (m/s)
f_g = ratio of antenna impedance to free space impedance, unitless (200/377)
V = source voltage.

For the Para-IRA, τ = 2, assuming a perfect balun design for a 50-Ω to 200-Ω impedance transition. The maximum source voltage divided by the risetime can approximate the derivative of the source voltage, *dV/dt*. Simplifying the above equation with the above values and approximations, we have

$$E_{rad} = \frac{1.7\times10^{-9}}{r}\,\frac{V_{\max}}{risetime}$$

where:

$V_{\max}$ = maximum source voltage (volts)
risetime = pulse risetime (seconds).

6.2 Antenna Pattern

We calculate now the radiated field off-boresight for the antenna, in order to determine the antenna beamwidth and the spot size on the ground. The mathematical details are a bit long, but the technique has already been described in [3]. The theory is based on a high-frequency approximation of the integral of the electric field over the aperture. The resulting fields are provided in Figure 6.1, for both the E-plane (top) and the H-plane (bottom). The field strength in this figure is derived from a 500 V, 250 ps pulse. We can see that the time domain field has a peak on boresight, and as one goes further off boresight, the radiated impulse is reduced in magnitude and longer in duration. These patterns show that the half field half beamwidth (HFHBW) is about 7° in the H-plane and 10° in the E-plane. Thus, with feed arms at ±45°, we get a slightly fan-shaped beam. (Note that the full beamwidth is twice these numbers.) With feed arms located at ±30°, we have demonstrated that the beamwidths become approximately equal in both planes [4], so it is reasonable to estimate that the half beamwidth is the average of the two beamwidths, or about 8.5° in both planes. Therefore, the full beamwidth is 17° in both planes with feed arms at ±30°.

We wish now to determine whether the calculated beamwidth is sufficient to create a 100-meter radius spot size on the ground. Since we are radiating from a height of 500 meters, we will need an antenna pattern with a half beamwidth of 11.3°. So our estimate of 8.5° half beamwidth is a little narrower than we would like. The simplest way of fixing the problem is to defocus the antenna slightly, which has the additional effect of reducing the field on boresight. Since we can easily generate larger signal boresight by increasing transmitter output, the loss of some field magnitude on boresight will not be a problem. Alternatively, we could operate the Para-IRA at a height of 650 meters, instead of 500 meters. This would reduce the field on boresight by a factor of 500/650 = 0.77, which again will be easily made up by a more powerful transmitter.

Finally, we note that the actual shape of the reflector will have some deviation from the ideal shape. Thus, we are going to get a slight defocusing effect due to the imperfections in the fabrication and due to the stretch that occurs when the fabric is under stress. So we may not have to do anything to defocus the antenna – it may just happen on its own.

6.3 Frequency Range

We calculate now the lower and upper ends of the frequency range for the proposed Para-IRA. The lower frequency response, f_L, of the Para-IRA is calculated in [5] as:

$$f_L = \frac{c}{4\pi F}$$

where:

f_L = lower frequency response (Hz)
$c = 3 \times 10^8$ (m/s)
F = focal length (m).

For the prototype, with a focal length of four feet (1.22 m), the lower frequency response is 20 MHz. So there is plenty of low-frequency range available with this antenna.

The upper frequency response is limited by the surface tolerance of the antenna reflector. The CIRA is made from the same metallized mesh as the Para-IRA, but it is supported on a rigid frame. The CIRA has a surface tolerance of about ± 1 cm, and we measured the upper frequency limit of the CIRA as about 10 GHz. For the Para-IRA, with no rigid supporting structure, the deviation from a perfect parabola will be greater – perhaps around ± 2.5 cm. By scaling the frequencies, we estimate that the high-frequency response of the Para-IRA will be about 4 GHz. This should easily cover our frequency range of interest.

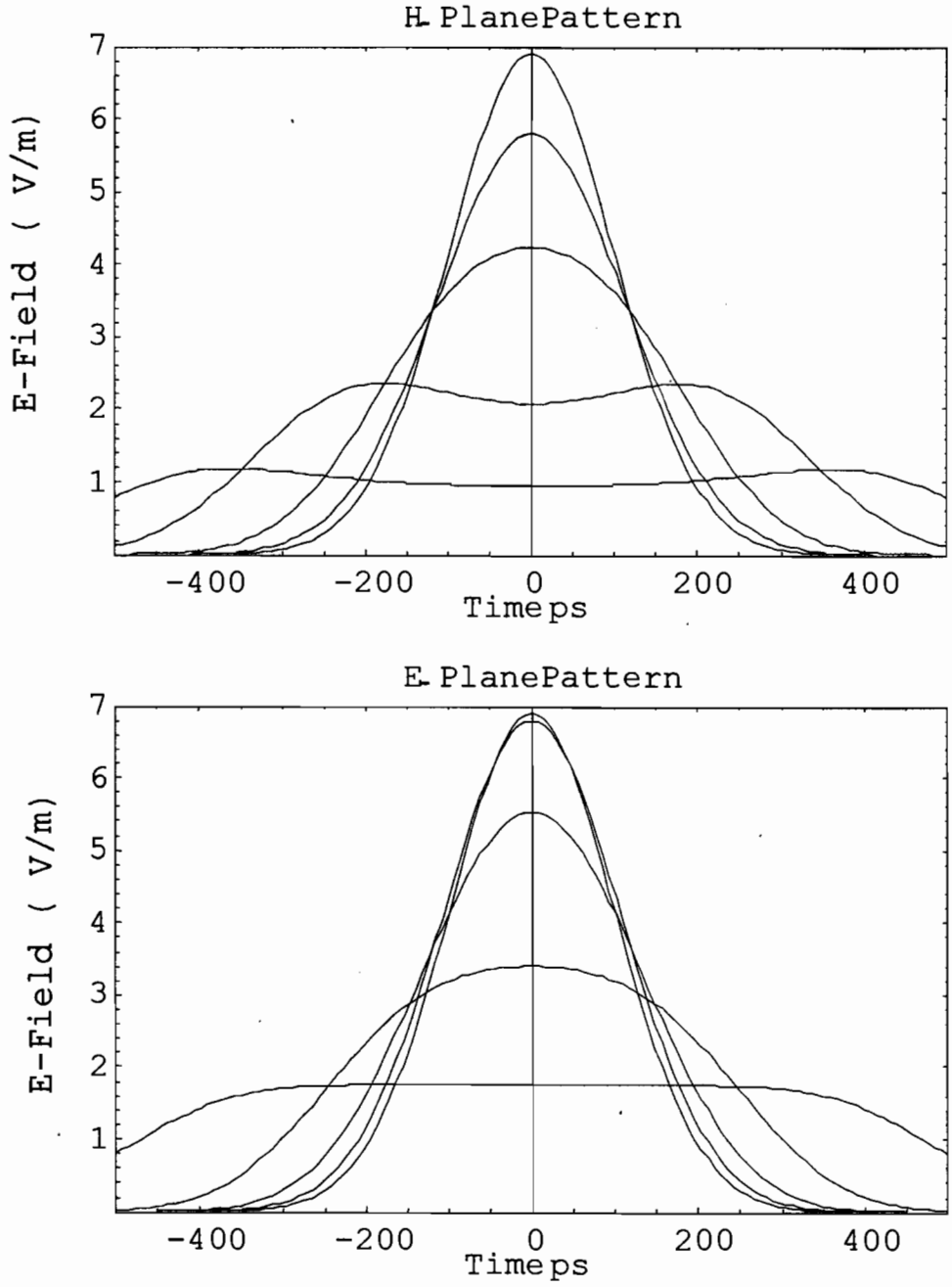

Figure 6.1. Radiated field in the H-Plane (top) and E-Plane (bottom) for the Para-IRA with a 4-foot (1.22 m) diameter, with feed arms at ±45°, observed at a distance of 500 m, driven by a 500 V pulser with risetime of 250 ps.

6.4 Aperture Shaping

Next, we consider how one might improve the prompt response by shaping the reflector. The far field is determined by the *y*-component of the electric field everywhere in the aperture. For most of the aperture, the *y*-component of the electric field is all oriented in the same

direction. However, for a portion of the aperture, the y-component of the electric field is oriented in the opposite direction. If one could eliminate the areas of the aperture where E_y is oriented in the wrong direction, the prompt radiated response from the IRA would be improved. To find these areas of negative field contribution, we first calculate the electric field in the aperture. We do this by solving the Laplace equation for the TEM feed structure and then by taking the gradient of the resulting electric potential.

The portion of the aperture that contributes negatively to the radiated field is shown in Figure 6.2. The portion of the aperture above the heavy line makes a negative contribution to the radiated field. Thus, over that portion of the aperture, we would ideally replace the conducting reflector with a non-conducting fabric, in order to improve performance.

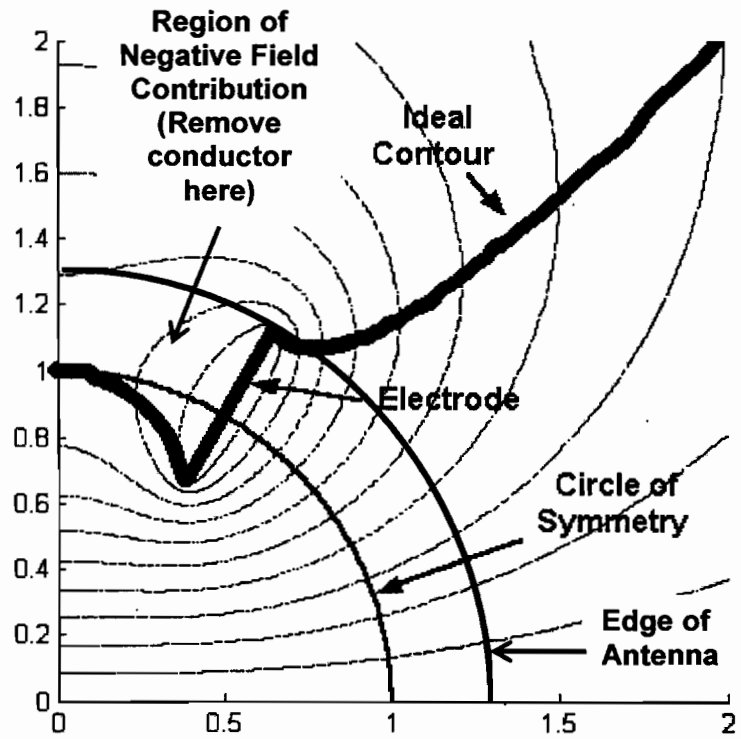

Figure 6.2. Sketch of the aperture fields of an one-quarter of an IRA reflector. Note the Region of Negative Field Contribution, where conductor in the reflector should be removed.

Dr. J. Scott Tyo [6] provided us with the results of theoretical calculations for eight IRA configurations: 45-degree arms, with and without the circle of symmetry coinciding with the edge of the reflector; and 30-degrees arms, with and without the circle of symmetry coinciding with the edge of the reflector. The results of these calculations are shown below in Table 6.1.

Table 6.1. Computation of the resultant field for IRAs (h_a/a) with and without the negatively contributing reflector area.

	Circle of Symmetry Coincides with the Charge Center of the Feed Arms (Arms overhang the reflector edge)		Circle of Symmetry Coincides with the Outer Edge of the Feed Arms (Outer Edge of arms match edge of reflector)	
	Complete Reflector	Negatively Contributing Area Removed	Complete Reflector	Negatively Contributing Area Removed
Arms 45° from vertical	0.6482	0.6636	0.6193	0.6875
Arms 30° from vertical	0.7363	0.7451	**0.6804**	**0.7368**

Our Para-IRA is the case with the arms ±30° from the vertical, with the circle of symmetry coinciding with the outer edge of the feed arms. Thus, by removing the negatively contributing region, we expect to see an increase in field strength from 0.6804 to 0.7386 or 8.6%.

6.5 Far Field Determination

We calculate now the range length required in order to test the Para-IRA in the far field. The two antennas should be separated by a distance of

$$r \geq \frac{3}{2}\frac{a^2}{c t_r}$$

where:

r = distance between the antennas (m)
a = radius of the reflector (m)
c = speed of light (m/s)
t_r = risetime of the radiated pulse (picoseconds).

The radius of the Para-IRA is 0.61 m and the risetime of the convolved integrated Gaussian pulse is 250 ps, thus the far field starts at about 7.4 meters. We acquired all field measurements for the Para-IRA at 9.5 meters distance from the source, thus ensuring that we were in the far field for the 250 ps risetime Gaussian pulse. Note, however, that the data was taken at a faster risetime, so results above a certain frequency are in the near field.

7. Testing

7.1 Time Domain Antenna Range Description

Figure 7.1 shows the Farr Research time domain antenna range instrumentation. The range functions analogously to its more common frequency domain counterpart, only in the time domain. The sensor radiates a pulse – a derivative of the step created by the 20-ps risetime step generator. The antenna under test (AUT), in this case the Para-IRA, receives the pulse. The received pulse is recorded on the Tektronix TDS8000 sampling oscilloscope. We then deconvolved the frequency response of instrumentation and the source, leaving the frequency response of the AUT. This is the impulse response in the time domain. We then can convolve any arbitrary wave shape (e.g. a 250-ns Gaussian pulse) with the impulse response, in order to calculate the field radiated in response to an arbitrary source.

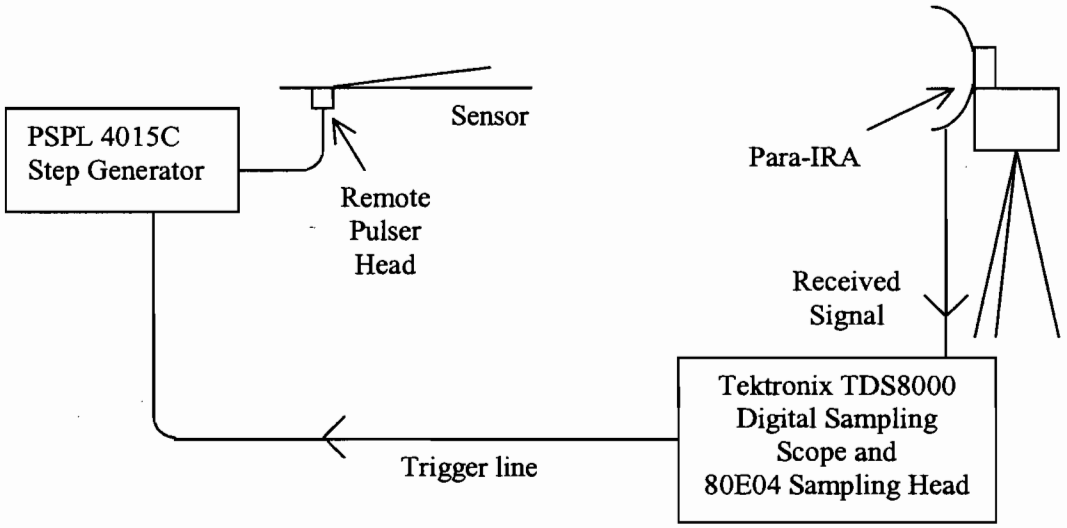

Figure 7.1. Time-domain antenna range measurement system.

7.2 Field Strength on Boresight

The field radiated on bore sight can be calculated from [7] as

$$\frac{E_{rad}(t)}{\sqrt{Z_o}} = \frac{1}{2\pi rc} h_N(t) \circ \frac{1}{\sqrt{Z_c}} \frac{dV_{src}(t)}{dt}$$

where the " ∘ " symbol indicates convolution, and

$E_{rad}(t)$ = radiated field on boresight (V/m)
Z_o = free space impedance (ohms)
r = distance to the observation point on boresight (meters)
c = speed of light (m/s)
h_N = normalized impulse response (m/s)
Z_c = impedance of input cable (ohms) – usually 50 Ω
$V_{src}(t)$ = source input voltage.

Using this equation and the normalized impulse response, we calculate the peak boresight field strength as a function of distance from the Para-IRA. Figure 7.2 shows the results.

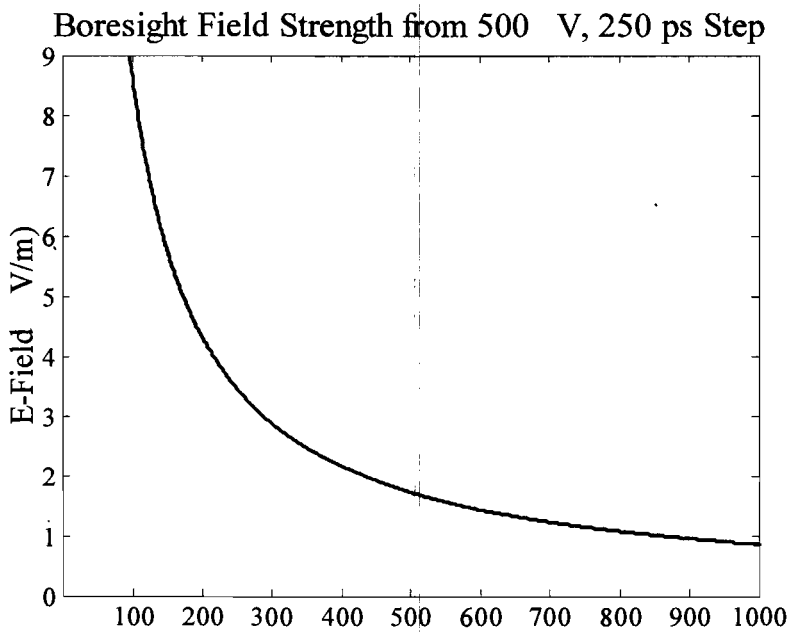

Figure 7.2. Peak field strength along boresight.

We note that the field strength is less than our original predictions. We predicted 6.8 V/m at 500 meters, but the above measurements give us about 1.7 V/m. We attribute at least some of the decrease to the broadening of the beamwidth, discussed in Section 7.5. The discrepancy may also be due to a small amount of wrinkling of the reflector surface. It may also be due to the longer *F/D* ratio of the reflector.

7.3 Normalized Impulse Response

Figure 7.3 shows the normalized boresight impulse response, $h_N(t)$, as function of time and frequency.

7.4 Para-IRA Effective Gain on Boresight

Figure 7.4 shows the effective gain of the Para-IRA on boresight as a function of frequency.

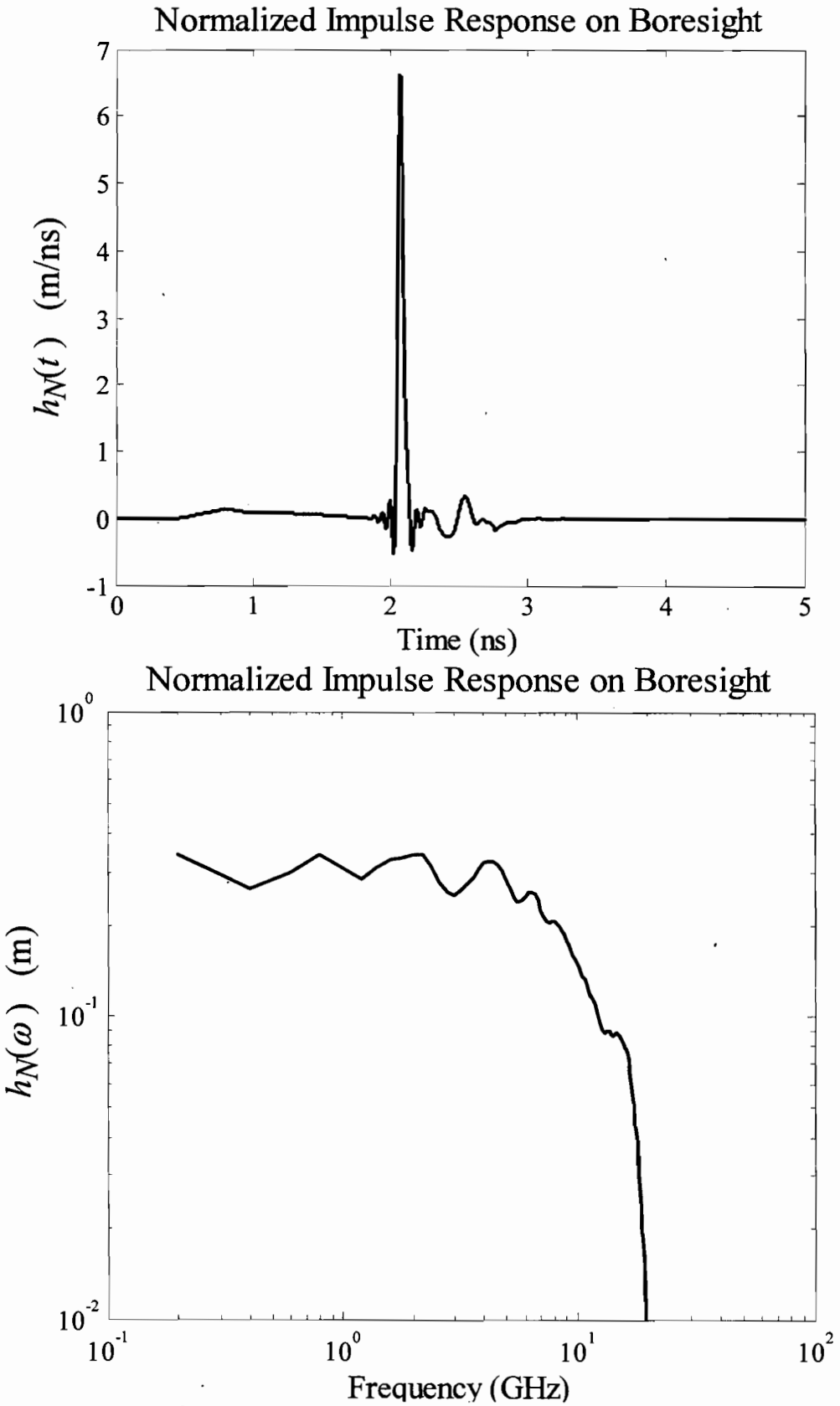

Figure 7.3. Boresight normalized impulse response.

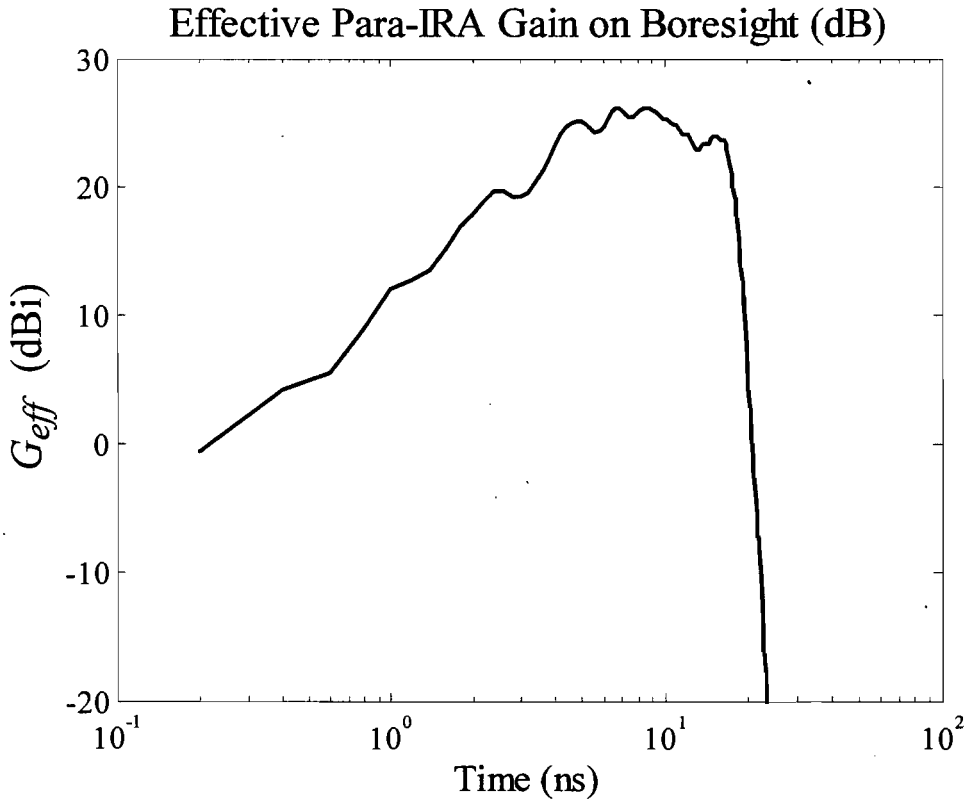

Figure 7.4. Effective Gain of the Para-IRA on Boresight.

7.5 Antenna Pattern

7.5.1 Peak Pulse Field Pattern

We measured the half-field half-beamwidth (HFHBW) pattern of the Para-IRA using the techniques above. We rotated the Para-IRA in one-degree increments, from boresight to twenty degrees off boresight, in both the E- and H-planes. We calculate at each angle the normalized impulse response, $h_N(t)$, and convolve it with a 250-ps Gaussian pulse. The convolution of the $h_N(t)$ obtained at each angle with the Gaussian produces the field strength at that angle. The peak field strength is then normalized to the boresight field strength and is plotted against the antenna angle in Figure 7.5.

The field strength falls off much as expected, as Figure 7.5 shows, with only a slightly wider pattern than our original prediction. The measured HFHBW is approximately 11 degrees in the H-plane and 12 degrees in the E-plane, compared to the predicted estimate of 8.5 degrees both planes. We attribute the wider pattern to the deviation of the physical, fabric antenna from the ideal model used for the calculations.

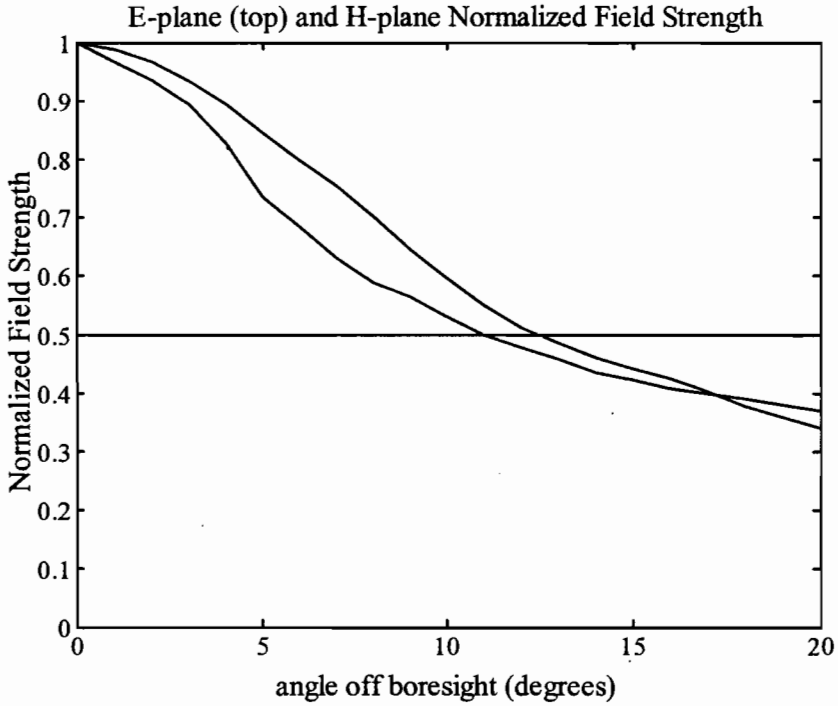

Figure 7.5. Para IRA Beamwidth.

7.5.2 Effective Gain Pattern

Figures 7.6 and 7.7 show the effective gain of the Para-IRA for six frequencies plotted against the angle off boresight. From the top trace down, the frequencies are: 4, 2, 1, 0.8, 0.4 and 0.2 GHz. No frequencies higher than 4 GHz are plotted since, at that frequency, the variations in the fabric of the antenna degrade the frequency response. In addition, at that frequency the spectral content of a 250-ps HFHBW Gaussian pulse is down from the maximum by approximately 30 dB, so there will be negligible source signal there.

7.6 Effective Gain vs. Frequency and Angle

Using the same raw data as above, we plotted the effective gain of the Para-IRA as a function of frequency and angle. The resulting color plots are provided in Figures 7.8 and 7.9. As expected, the plots show that the Para-IRA's highest effective gain is between about 1 and 12 GHz.

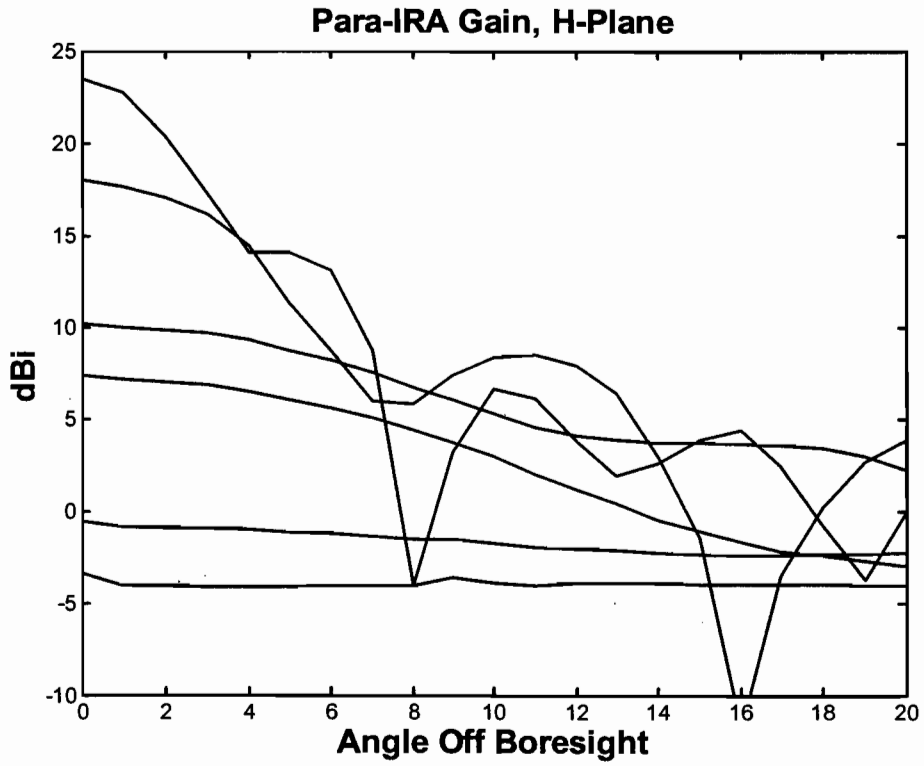

Figure 7.6. Effective gain of the Para-IRA in the H-Plane for 4, 2, 1, 0.8, 0.4 and 0.2 GHz.

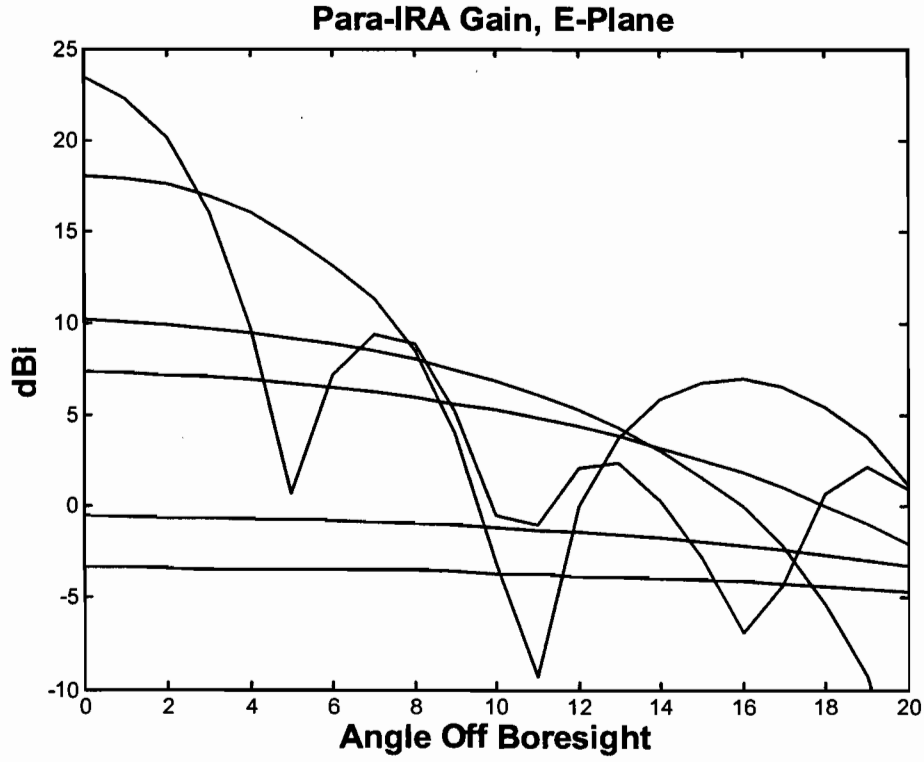

Figure 7.7. Effective gain of the Para-IRA in the E-Plane for 4, 2, 1, 0.8, 0.4 and 0.2 GHz.

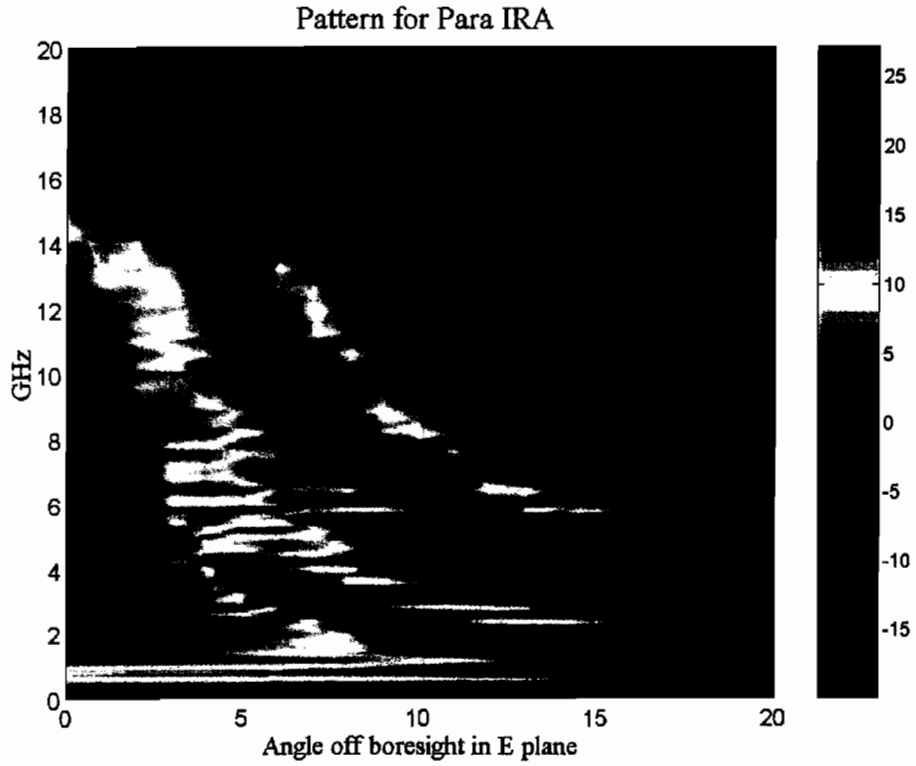

Figure 7.8. Effective gain of the Para-IRA in the E-plane.

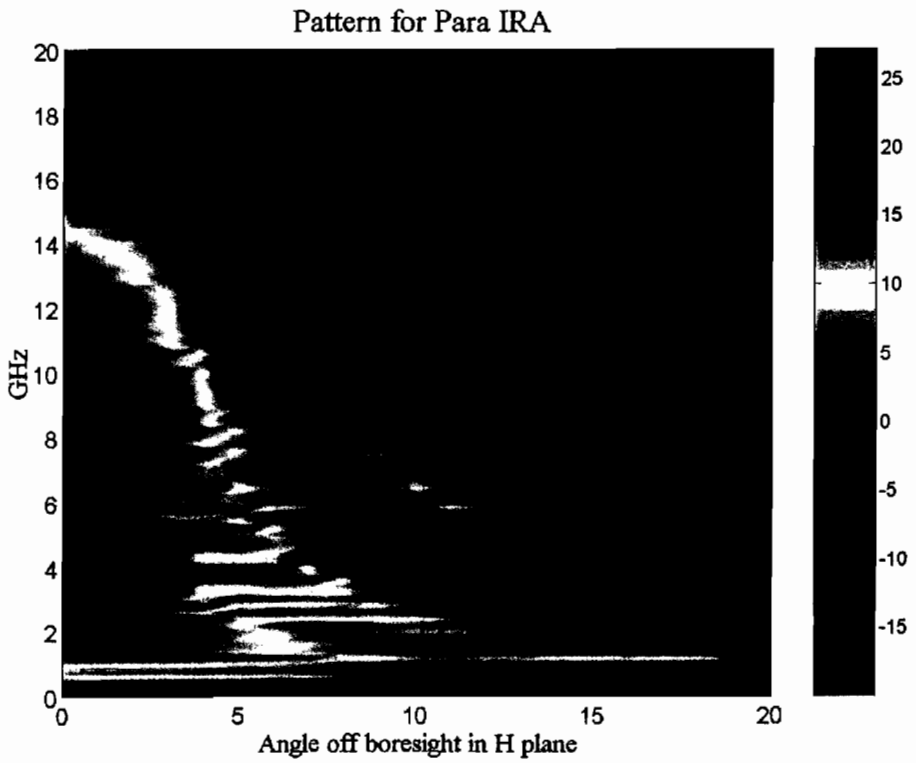

Figure 7.9. Effective gain of the Para-IRA in the H-plane.

7.7 Inflation Test

We configured the Para-IRA into an inflatable version, in order to test the boresight antenna response. We did this in order to try testing the Para-IRA electrically, without using an expensive wind tunnel. Therefore, we used only inexpensive equipment to generate air pressure to shape the reflector.

Figure 7.10 shows the measurement setup. We removed the Para-IRA from its wooden frame and attached it to a polycarbonate ring at twelve peripheral points with Velcro straps. The reflector was stretched loosely to allow the air pressure to form it into a parabolic shape. We then enclosed the Para-IRA in 1-mil thick (0.0254 mm) plastic sheet taped to the edge of the reflector. We inflated the resulting balloon with a common floor fan. Since the inflated reflector was physically close to the accurate parabolic frame, we could compare the shape of the inflated reflector to a known parabola. This comparison showed a fairly good match. The reflector was only somewhat less curved than the frame, and the shape could be improved with more air pressure.

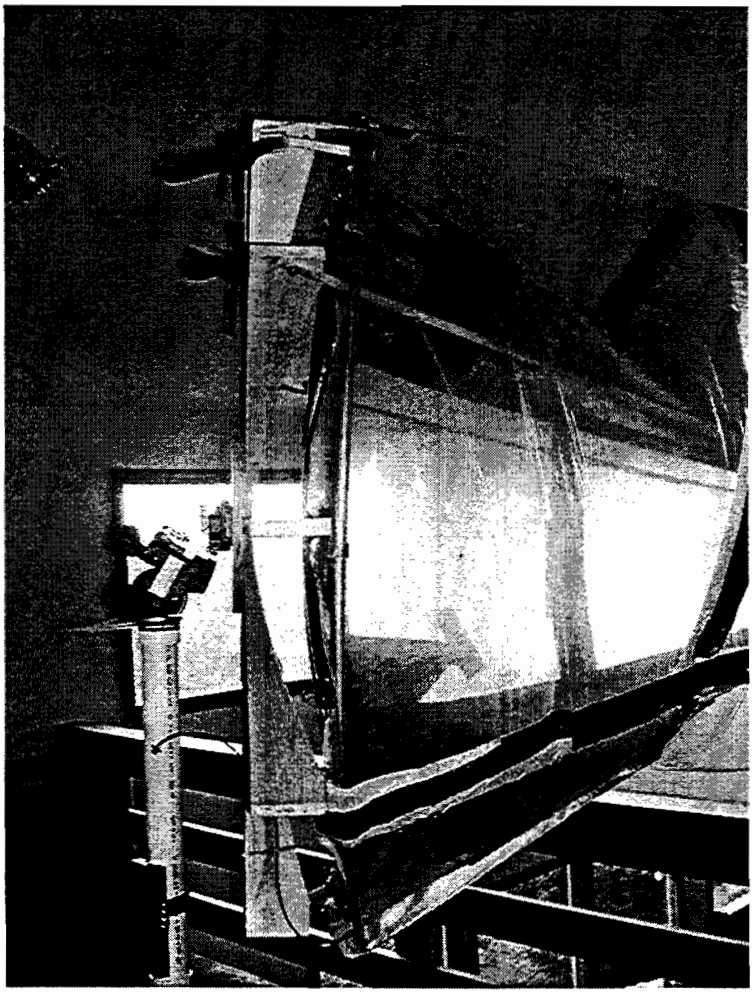

Figure 7.10. Reflector encased in airbag.

Figure 7.11 shows four raw voltage traces of the radiated boresight field measured during the inflation experiment. From left to right, and smallest to largest, the traces are the recorded raw voltage with the fan off, on low, on medium and on high.

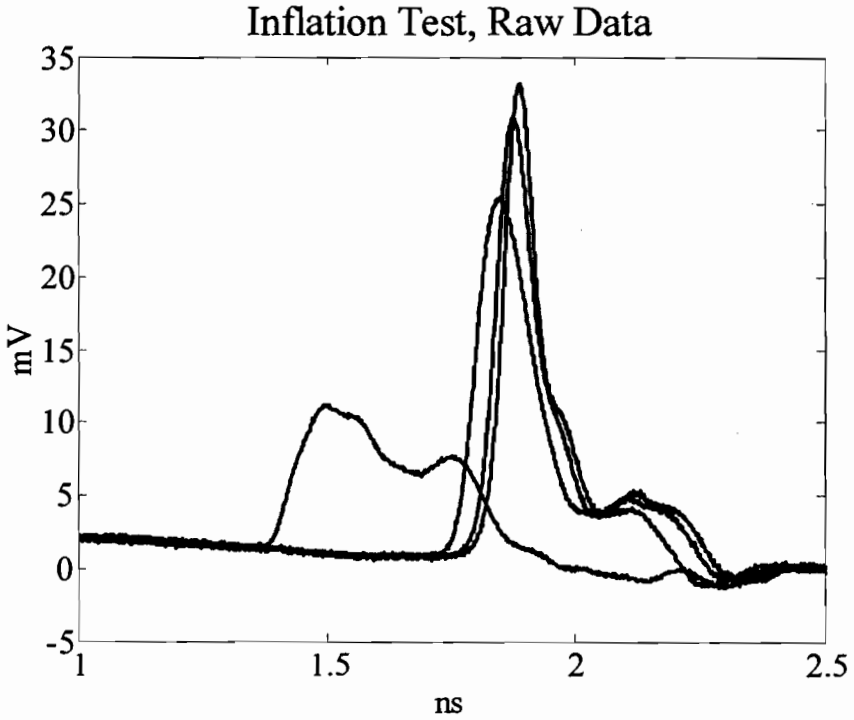

Figure 7.11. Voltage on boresight for inflation test.

From this figure we see the received field strength increases as the air pressure on the reflector increases. The maximum raw voltage recorded is approximately sixty percent of the voltage recorded with the reflector mounted on an accurate parabolic frame.

7.8 Aperture Shaping Test

We investigated modifying the aperture shape to increase the radiated field strength as discussed in section 6.4. We removed the material that contributes negatively to the field strength using the technique discussed in Section 6.4. Figure 7.12 shows the reflector after the negatively contributing area of the reflector was cut out.

Figure 7.13 shows a comparison of the boresight received raw voltage before and after the negatively contributing material was removed. For both measurements, the azimuth and elevation of the Para-IRA were adjusted for maximum signal strength, to reduce the possibility of alignment error.

The lower trace in Figure 7.13 is the baseline boresight measurement made before the material was removed. The top trace is the boresight measurement after the material was removed. The difference between the two levels is well within the measurement repeatability error.

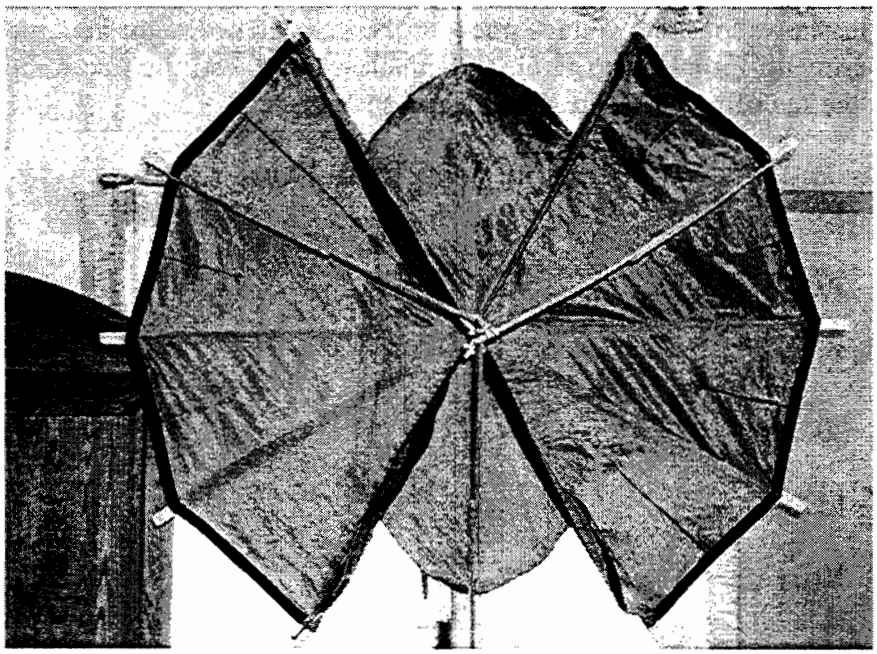

Figure 7.12. Para-IRA with region of negative field contribution removed.

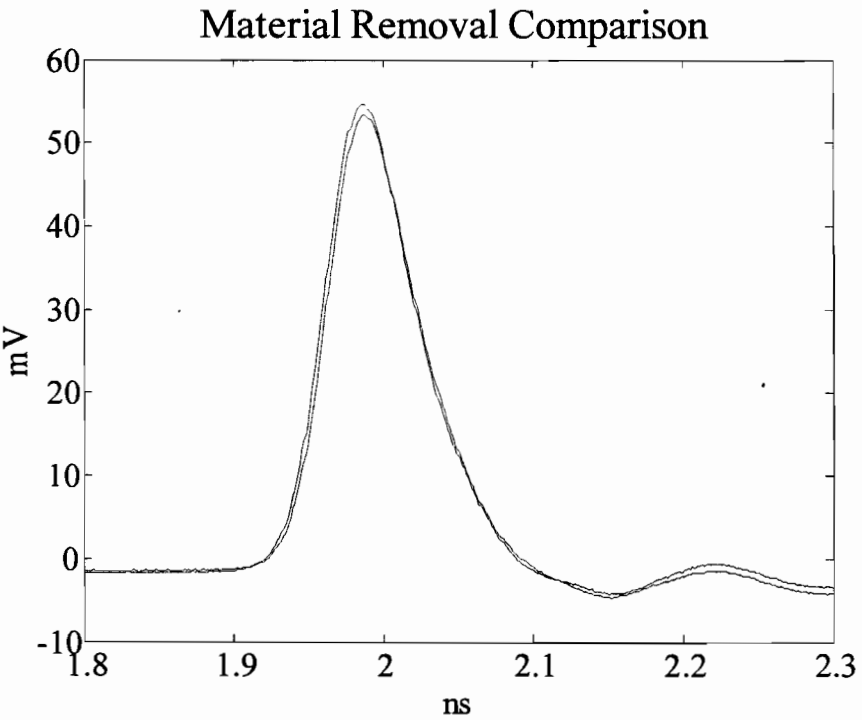

Figure 7.13. Evaluation of removal of material contributing to negative field.

7.9. Tow Test

The Phase I Tow Test consisted of towing the Para-IRA and parachute behind a moving vehicle. We photographed the reflector and parachute canopy to estimate the Para-IRA's shape

during flight. In addition, we measured the force on the Para-IRA as a function of speed, to determine the Para-IRA's descent rate. Using the results of the tow test, we should be able to modify the reflector shape to improve its fidelity to a parabola under wind load. Later, we may try to simulate the reflector shape, either with air pressure or with a static frame, in order to measure the antenna pattern under simulated wind-loaded conditions.

Figure 7.14 is a photograph of the tow test underway. A 6-foot stepladder is secured to the pickup bed, and this ladder supports a board with pulleys at either end. A rope is connected from the parachute through the two pulleys, to a scale, which is secured to the bed of the truck. The scale is calibrated in one-pound (4.45 nt) increments to 100 lbs (445 nt). The force generated by wind pressure is read from this scale and is recorded as a function of vehicle speed. This photograph was taking at a vehicle speed of about 30 mph (48 kph). Note that the parachute has not been fully opened. We made all force measurements with the Para-IRA fully opened by using the polycarbonate ring.

Figure 7.14. Para-IRA tow test in progress, at 30 mph (48 kph).

We have plotted the force on Para-IRA as a function of vehicle speed in Figure 7.15. Note that the indicator on the scale can vibrate somewhat, so the measurements have an error margin of around ±2 pounds (9 nt). We suspect that the last measurement in the graph may be spurious, because we expect the curve to be smooth. This possibly spurious result may be due to excessive vibration.

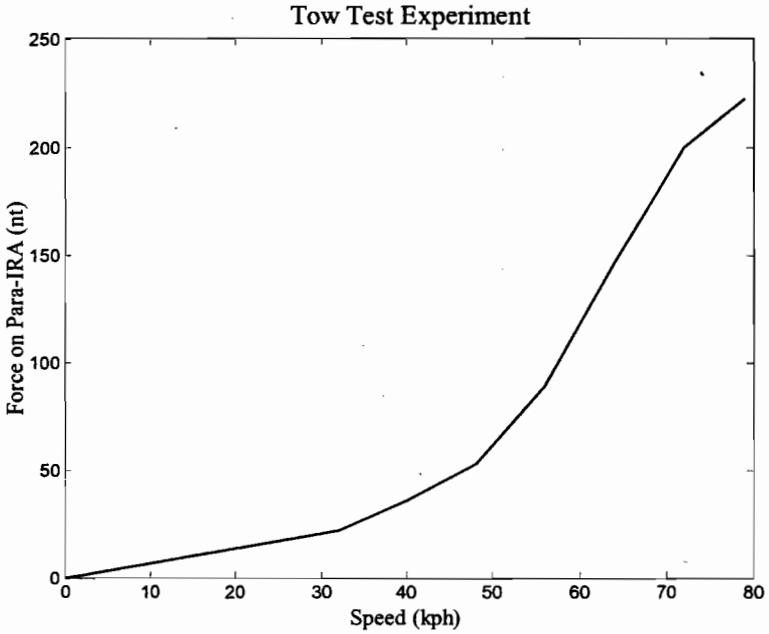

Figure 7.15. Force on the Para-IRA vs. tow truck speed.

Based on these results, we find that a 50-pound (23 kg, 222 nt) package will have a descent rate between 70 and 80 kph. Our estimate of $k = 0.6$ in the equation for the descent velocity of parachute resulted in a prediction of 50 kph. Given a measured descent rate of approximately 75 kph, we can adjust the k for this particular parachute to about 0.25. Note, however, that more recent estimates of the source weight are closer to 20 lb (89 nt), which would suggest a descent rate near 58 kph.

Figure 7.16 shows the Para-IRA fully opened with the reflector inflated. There is no polycarbonate ring used for this photograph – the only force shaping the Para-IRA is air pressure. The tow-truck speed was about 40 mph (64 kph). At this speed, the Para-IRA is well inflated, and it forms a smooth surface. However, the white reefing line is clearly visible, and tends to form arcs rather than straight line segments. We attribute this cupping effect to the fact that the force on the reflector perimeter is aligned with the parachute lines rather than pointed radially outward. The parachute lines tend to pull the reflector edge in at the tie-points, while the air pressure forces the center of the gores out, thus creating the cupping effect.

The tendency of each gore of the Para-IRA to cup can be reduced or eliminated by one of several methods. First, we can lengthen the short lines that tie the reflector perimeter to the parachute skirt. This may allow the parachute to open to a greater diameter. In addition, we may also need to use a parachute with a larger diameter. The longer reflector tie lines would then pull radially outward, rather than towards the junction of all the parachute lines. Finally, it may be helpful to make the reflector more permeable to air, in order to reduce the force normal to the reflector. This could be implemented either by using a reflector fabric with a more sparse mesh, or by introducing some holes into the reflector.

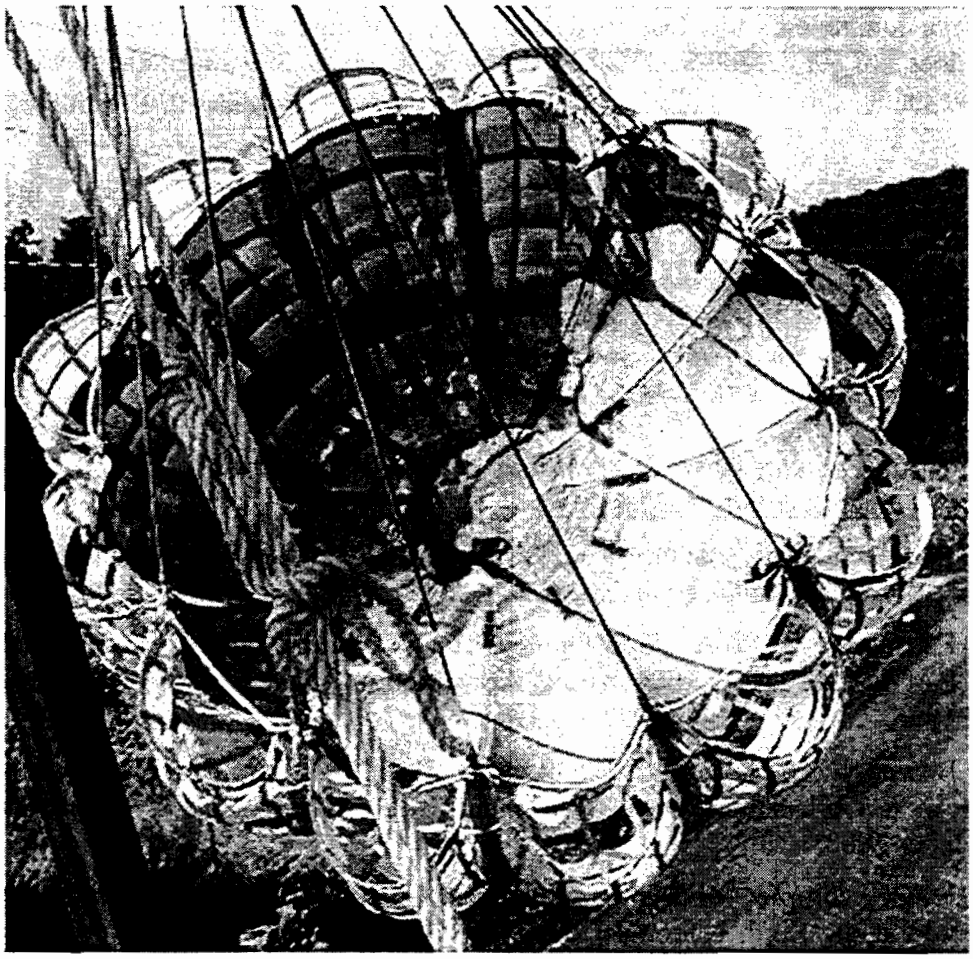

Figure 7.16. Para-IRA inflated during 40 mph (64 kph) tow test.

8. Conclusions

We have fabricated and tested two prototype Para-IRAs: one for electromagnetic testing and one for mechanical testing. The results of these tests suggest that the Para-IRA may be a viable concept to develop as a parachute deployable antenna and transmitter.

Our collaboration with Irvin Aerospace has verified that the reflector and feed system can be adapted to a parachute and packaged in a conveniently small size. Calculations made by Irvin Aerospace show that parachute size and descent rate are well within acceptable limits.

We have tested the Para-IRA on our antenna range at low voltage. The results indicate that the full-scale version will deliver a peak field strength of around 1.7 kV/m at a distance of 500 m above the ground, based on a 500 V, 250-ps risetime pulse generator. The full-scale device will deliver an electric field of at least 1 V/m over a radius on the ground of nearly 100 meters. The field strength measured here is somewhat lower than our predictions, perhaps due to a small amount of wrinkling of the reflector surface or the longer *F/D* ratio of the reflector.

We have conducted a tow test on an early model of the Para-IRA, where we learned that the reflector does not yet deploy to the desired parabolic shape. Several methods were proposed to improve the shape, and they will be investigated during the next phase of this investigation.

References

Note: Sensor and Simulation Notes and Transient Radiating Antenna Memos are published by the Air Force Research Laboratory, Directed Energy Directorate. They are available from the authors or from the editor of the series, Dr. Carl E. Baum, AFRL/DE, Building 909 3550 Aberdeen Ave. SE, Kirtland AFB, NM 87117

1. Jean Potvin. *Calculating the Descent Rate of a Round Parachute.* http://www.pcprg.com/rounddes.htm.
2. E. G. Farr and C. E. Baum, "Time Domain Characterization of Antennas with TEM Feeds", *Sensor and Simulation Note* 426, October 1998.
3. E. G. Farr and C. A. Frost, "Development of a Reflector IRA and a Solid Dielectric Lens IRA, Part I: Design, Predictions and Construction", *Sensor and Simulation Note* 396, April 1996.
4. L. H. Bowen, E. G. Farr, *et al*, "Experimental Results of Optimizing the Location of Feed Arms in a Collapsible IRA and a Solid IRA", *Sensor and Simulation Note* 450, November 2000.
5. E. G. Farr, Simple Models of Antennas Useful in Ultra-Wideband Applications, presented at the Sixth National Conference on High Power Microwaves, San Antonio, August 1992. Also published as Transient Radiating Antenna Memo 2.
6. J. Scott Tyo, Personal communication with E. G. Farr, May 2001.
7. E. G. Farr, C. E, Baum, Time Domain Characterization of Antennas with TEM Feeds, *Sensor and Simulation Note* 426, October 1998.

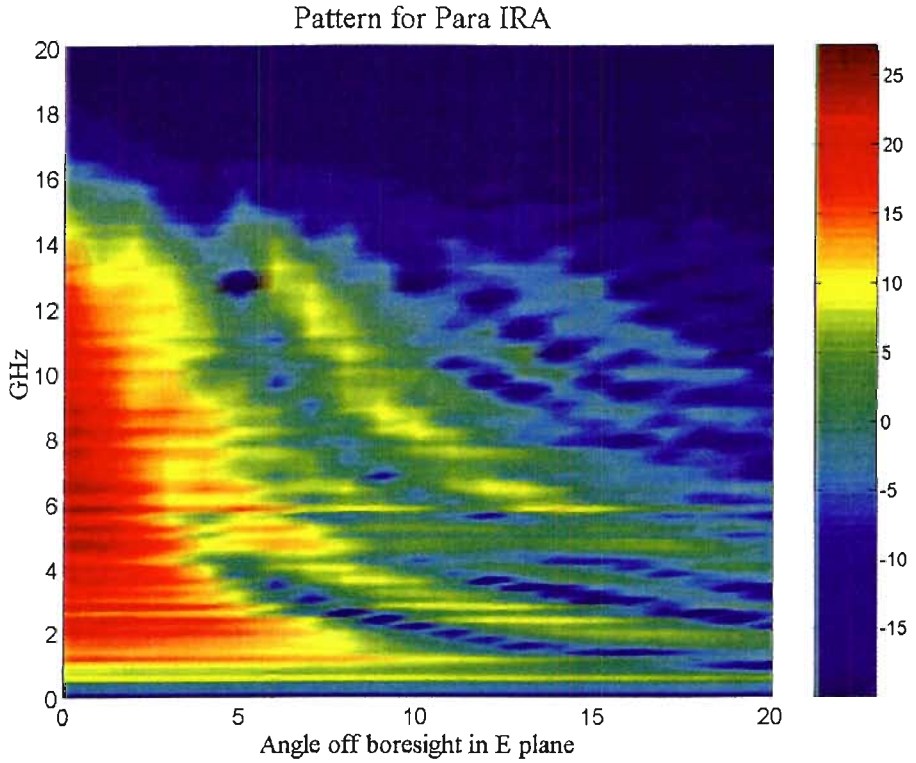

Figure 7.8. Effective gain of the Para-IRA in the E-plane.

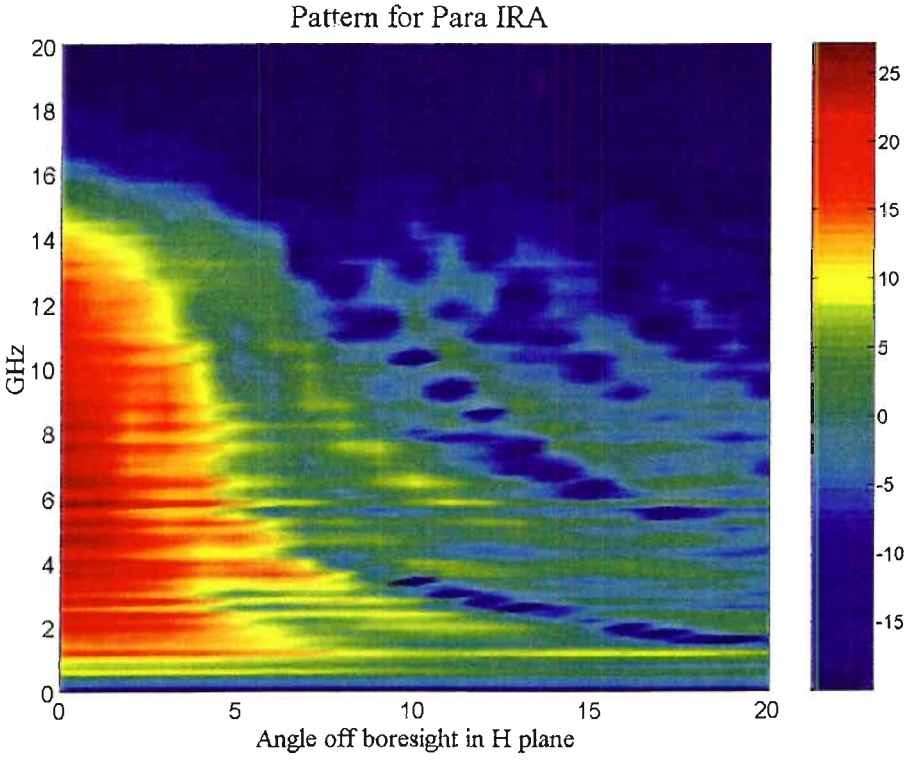

Figure 7.9. Effective gain of the Para-IRA in the H-plane.